Hierarchically Assembled Porous ZnO Nanoparticles: Synthesis, Surface Energy, and Photocatalytic Activity

Fen Xu,[†] Peng Zhang,[†] Alexandra Navrotsky,*[,†] Zhong-Yong Yuan,[‡] Tie-Zhen Ren,[‡] Matej Halasa,[‡] and Bao-Lian Su*[,‡]

NEAT ORU and Peter A. Rock Thermochemistry Laboratory, University of California at Davis, One Shields Avenue, Davis, California 95616, and Laboratory of Inorganic Materials Chemistry, University of Namur (FUNDP), 61 rue de Bruxelles, B-5000 Namur, Belgium

Received May 2, 2007. Revised Manuscript Received July 25, 2007

We show an effective experimental method to prepare hierarchically porous zinc oxide (ZnO) spherical nanoparticles through a self-assembly pathway using surface-modified colloidal ZnO nanocrystallites as the building blocks and P-123 copolymers as the template in aqueous solution. Copolymers are thoroughly removed by Soxhlet extraction with ethanol and calcination at 400 °C. The final products have been characterized by X-ray powder diffraction (XRD) pattern, scanning electron microscopy (SEM), transmission electron microscopy (TEM), high-resolution TEM (HRTEM), and photoluminescence (PL) spectroscopy. On the basis of calorimetric measurements reported separately, the surface enthalpy (γ) of the hydrated porous ZnO is 1.42 ± 0.21 J/m^2, in good agreement with that of ZnO nanoparticles. The calorimetric results support the presence of self-assembled ZnO nanocrystallites in the nanoporous ZnO. Photocatalytic activitiy of porous ZnO nanoparticles has been tested on the photodegradation of phenol under ambient condition, indicating that porous ZnO nanoparticles show superior activity to TiO_2 nanoparticles (PC-500).

1. Introduction

Semiconductor photocatalysts offer huge potential for elimination of toxic chemicals.[1−4] Porous semiconductor photocatalysts are attractive in applications such as bioengineering and photocatalysis, through minimizing the distance between the site of photon absorption and electron/hole redox reactions to improve efficiency.[5−7] Semiconductor photocatalysts can be rendered porous in different ways, such as the selective leaching of one phase from two-phase composites to create porosity,[8,9] the utilization of regular channels in mesoporous silica as nanoreactors for producing pores,[10−15] and the use of sacrificial templates for pore formation (i.e., surfactant assemblies,[16] colloidal crystal templates,[17] and block copolymers[18−24]).

Zinc oxide (ZnO), with a wide band gap (3.37 eV) and large exciton binding energy (∼60 meV), has witnessed an explosion of interest in the past few years because of advances in synthesis and unique optoelectronic, catalytic, and photochemical properties.[25−30] There is recent emphasis

* Corresponding authors. E-mail address: anavrotsky@ucdavis.edu (A.N., main corresponding author); bao-lian.su@fundp.ac.be (B.-L.S.). Phone: (530) 752-3292. Fax: (530) 752-9307.

[†] University of California at Davis.

[‡] University of Namur (FUNDP).

(1) Hu, J. S.; Ren, L. L.; Guo, Y. G.; Liang, H. P.; Cao, A. M.; Wan, L. J.; Bai, C. L. *Angew. Chem., Int. Ed.* **2005**, *44*, 1269.
(2) Hoffmann, M. R.; Martin, S. T.; Choi, W. Y.; Bahnemann, D. W. *Chem. Rev.* **1995**, *95*, 69.
(3) Fujishima, A.; Honda, K. *Nature* **1972**, *238*, 37.
(4) Anpo, M.; Takeuchi, M. *J. Catal.* **2003**, *216*, 505.
(5) Jaramillo, T. F.; Baeck, S. H.; Kleiman-Shwarsctein, A.; McFarland, E. W. *Macromol. Rapid Commun.* **2004**, *25*, 297.
(6) Soler-Illia, G. J. A. A.; Crepaldi, E. L.; Grosso, D.; Sanchez, C. *Curr. Opin. Colloid Interface Sci.* **2003**, *8*, 109.
(7) Takahara, Y.; Kondo, J. N.; Takata, T.; Lu, D. L.; Domen, K. *Chem. Mater.* **2001**, *13*, 1194.
(8) Toberer, E. S.; Löfvander, J. P.; Seshadri, R. *Chem. Mater.* **2006**, *18*, 1047.
(9) Rajamathi, M.; Thimmaiah, S.; Morgan, P. E. D.; Seshadri, P. *J. Mater. Chem.* **2001**, *11*, 2489.
(10) Kaleta, W.; Nowinska, K. *Chem. Commun.* **2001**, *6*, 535.
(11) Zhu, K. K.; Yue, B.; Zhou, W. Z.; He, H. Y. *Chem. Commun.* **2003**, *1*, 98.
(12) Dickinson, C.; Zhou, W. Z.; Hodgkins, R. P.; Shi, Y. F.; Zhao, D. Y.; He, H. Y. *Chem. Mater.* **2006**, *18*, 3088.
(13) Wang, Y. Q.; Yang, C. M.; Schmidt, W.; Spliethoff, B.; Bill, E.; Schuth, F. *Adv. Mater.* **2005**, *17*, 53.
(14) Wang, Y. G.; Xia, Y. Y. *Electrochim. Acta* **2006**, *51*, 3223.
(15) Yue, W. B.; Zhou, W. Z. *Chem. Mater.* **2007**, *19*, 2359 and references therein.
(16) Beck, J. S.; Vartuli, J. C.; Roth, W. J.; Leonowicz, M. E.; Kresge, C. T.; Schmitt, K. D.; Chu, C. T. W.; Olson, D. H.; Sheppard, E. W.; McCullen, S. B.; Higgins, J. B.; Schlenker, J. L. *J. Am. Chem. Soc.* **1992**, *114*, 10834.
(17) Holland, B. T.; Blanford, C. F.; Stein, A. *Science* **1998**, *281*, 538.
(18) Zhao, D. Y.; Feng, J. L.; Huo, Q. S.; Melosh, N.; Fredrickson, G. H.; Chmelka, B. F.; Stucky, G. D. *Science* **1998**, *279*, 548.
(19) Deshpande, A. S.; Pinna, N.; Smarsly, B.; Antonietti, M.; Niederberger, M. *Small* **2005**, *1*, 313.
(20) Bosc, F.; Ayral, A.; Albouy, P. A.; Datas, L.; Guizard, C. *Chem. Mater.* **2004**, *16*, 2208.
(21) Yuan, Z. Y.; Ren, T. Z.; Su, B. L. *Adv. Mater.* **2003**, *15*, 1462.
(22) Ren, T. Z.; Yuan, Z. Y.; Su, B. L. *Chem. Commun.* **2004**, *23*, 2730.
(23) Ren, T. Z.; Yuan, Z. Y.; Azioune, A.; Pireaux, J.-J.; Su, B. L. *Langmuir* **2006**, *22*, 3886.
(24) Chane-Ching, J.-Y.; Cobo, F.; Aubert, D.; Harvey, H. G.; Airiau, M.; Corma, A. *Chem.—Eur. J.* **2005**, *11*, 979.
(25) Wei, A.; Sun, X. W.; Xu, C. X.; Dong, Z. L.; Yang, Y.; Tan, S. T.; Huang, W. *Nanotechnology* **2006**, *17*, 1740.
(26) Vayssieres, L.; Keis, K.; Hagfeldt, A.; Lindquist, S. E. *Chem. Mater.* **2001**, *13*, 4395.
(27) Huang, M. H.; Mao, S.; Feick, H.; Yan, H. Q.; Wu, Y. Y.; Kind, H. Weber E.; Russo, R.; Yang, P. D. *Science* **2001**, *292*, 1897.
(28) Pan, Z. W.; Dai, Z. R.; Wang, Z. L. *Science* **2001**, *291*, 1947.
(29) Kong, X. Y.; Ding, Y.; Yang, R.; Wang, Z. L. *Science* **2004**, *303*, 1348.
(30) Gao, P. M.; Ding, Y.; Mai, W. J.; Hughes, W. L.; Lao, C. S.; Wang, Z. L. *Science* **2005**, *309*, 1700.

10.1021/cm071190g CCC: $37.00
Published on Web 10/19/2007

on developing porous ZnO nanostructures for optimized performance of dye-sensitized photovoltaic cells, hydrogen storage, catalysis, and secondary batteries.[26−31] So far, porous ZnO has been synthesized by several methods, such as dip-coating with a polystyrene (PS) template[32] or a copolymer gel template,[33] combinatorial electrochemical synthesis,[5] thermal oxidation of a ZnS precursor,[34] in situ precipitation using poly(acrylic acid) (PAA) membranes,[35] exotemplating with mesoporous carbon,[36] or in situ hydrolysis of $Zn(Ac)_2 \cdot 2H_2O$ in LiOH−ethanol solution combined with templating anneal of mesoporous precursors.[37] Rather than conventional nucleation and growth, assembly of nanoclusters provides an alternative mechanism for crystal growth. This work explores an easy method to produce porous ZnO nanocrystals on a large scale, through a self-assembly pathway in aqueous solution using surface-modified colloidal ZnO nanocrystallites as the building blocks and P-123 copolymers as the template. The as-prepared samples are characterized by various techniques for phase identification and optical properties. The synthetic pathway is interpreted in terms of the measured surface energies of nanoporous and nanoparticle ZnO.[38] The calorimetric results confirm that porous ZnO nanoparticles can be fabricated by the self-assembly of colloidal ZnO nanoclusters. The preliminary photocatalytic activity of nanoporous ZnO is also tested on the decomposition of phenol under ambient conditions.

2. Experimental Methods

2.1. Chemicals and Synthesis. Zinc acetate dihydrate ($Zn(O_2CCH_3)_2 \cdot 2H_2O$), lithium hydroxide (LiOH), ethanol (CH_3CH_2OH), Pluronics P-123 BASF ($HO(CH_2CH_2O)_{20}(CHCH_3CH_2O)_{70}(CH_2CH_2O)_{20}OH$, designated $EO_{20}PO_{70}EO_{20}$), 2-aminoethanesulfonic acid (Taurine, $C_2H_7NO_3S$), phenol (C_6H_5OH), commercial ZnO powder (particle size probably between 500 and 1000 nm, 99.9%), and ZnO nanopowder (<100 nm) were purchased from Aldrich and used as received without further purification. Titania nanoparticles (TiO_2, PC-500, >99.5%) from Millenium were used in photocatalytic measurements. Reagent grade zinc oxide (ZnO) powder was obtained from Alfa Aescar and calcined at 950 °C overnight before use for calorimetric study. Deionzed water was used in all the syntheses. All glassware was cleaned with aqua regia, thoroughly rinsed with deionzed water, and dried before use.

A typical synthesis involved the functionalization of the premade colloidal ZnO nanocrystallites followed by their self-assembly under the assistance of copolymers. First, colloidal ZnO nanocrystallites were prepared by the hydrolysis of $Zn(Ac)_2 \cdot 2H_2O$ in the LiOH−ethanol solution.[39] Second, these ZnO colloids were mixed with taurine in deionzed water (molar ratio of taurine/ZnO = 1:1.4), and the pH value was adjusted to ∼5.0 with 1 M HCl, followed by vigorous stirring at 25 °C for 24 h. This mixture was marked as Solution A. Then, P-123 (3.0 g) was mixed with deionzed water (15 mL) at pH ∼ 5.0 and stirred at 25 °C for 24 h (Solution B). Finally, 10 mL of Solution A was added dropwise into 15 mL of Solution B under stirring. After 3 h stirring, the resulting mixture was transferred into a Teflon lined autoclave and heated at 70 °C for 3 days. The precipitate was filtered and purified by Soxhlet extraction with ethanol to remove the surfactant species and then dried in an oven at 40 °C. Finally, the sample was calcined at 400 °C for 5−7 h.

2.2. Characterization. The X-ray powder diffraction (XRD) pattern was recorded on a Philips PW 1820 diffractometer using Cu Kα radiation. N_2 adsorption analysis was carried out with a Micromeritics Tristar 3000 at −196 °C, and the samples were outgassed at 120 °C overnight before the measurements. The surface area was obtained by the Brunauer−Emmett−Teller (BET) method, and the pore size distribution was calculated from the desorption branch of the isotherm using the Barrett−Joyner−Halenda (BJH) method. Transmission electron microscopy (TEM) was carried out on a Philips TECNAI-10 microscope at 100 kV. The specimen for TEM observation was prepared by embedding in epoxy resin and ultramicrotoming and then mounting on a copper grid. High-resolution transmission electron microscopy (HRTEM) was performed with a JEOL 3010 transmission electron microscope at 300 kV. Room-temperature photoluminescence (PL) spectroscopy was performed by a PELS55-luminescence spectrophotometer (λ_{ex} = 325 nm, Xe lamp) with a filter centered at 235 nm.

2.3. Photocatalytic Measurements. The photocatalytic activity of the as-synthesized porous ZnO nanocomposites was tested by decomposing phenol in water at room temperature. A tubular quartz beaker (capacity ca. 125 mL) was used as the photoreactor. The reaction system contained 47 mg of porous ZnO nanomaterial and 50 mL of a dilute aqueous phenol solution (0.03 g/L), which was stirred in the dark for 30 min to reach adsorption equilibrium of phenol before being exposed to UV irradiation. This reactor was exposed to one UV lamp (Osram Eversun, L40/79 K, 40 W), and the reaction mixture was stirred during UV irradiation. The analysis of the residual phenol concentration in the reactor was performed with a PELS55-luminescence spectrophotometer at room temperature (λ_{ex} = 269 nm, Xe lamp). As a comparison, the photocatalytic activities of TiO_2 (TiO_2 PC-500), commercial ZnO powder, and ZnO nanopowders were also tested under the same experimental conditions.

3. Results and Discussion

3.1. Formation of Porous ZnO Nanoparticles. The XRD pattern (Figure 1) showed well-resolved peaks characteristic of crystalline ZnO. All the diffraction peaks could be indexed as wurtzite ZnO (space group *P*63*mc*, JCPDS Card No. 36-1451).[40] The size of the ZnO crystallite domains calculated by the Scherrer formula based on the (100) peaks is 19 ± 1 nm. The increase in the crystallite size on calcination is obvious from the decrease in the peak width when compared with the initial nanoparticles (XRD pattern not shown).

Figure 2a shows the nitrogen adsorption−desorption isotherms. They can be identified as type IV, which confirms the characteristics of mesoporous materials. However, due

(31) Yao, Z.; Postma, H. M. C.; Balents, L.; Dekker, C. *Nature* **1999**, *402*, 273.
(32) Liu, Z. F.; Jin, Z. G.; Li, W.; Liu, X. X. *J. Sol-Gel Sci. Technol.* **2006**, *40*, 25.
(33) Jiu, J. T.; Kurumada, K.; Tanigaki, M. *Mater. Chem. Phys.* **2003**, *81*, 93.
(34) Shan, C. X.; Liu, Z.; Zhang, Z. Z.; Shen, D. Z.; Hark, S. K. *J. Phys. Chem. B* **2006**, *110*, 11176.
(35) Xiao, Y. H.; Li, L.; Li, Y.; Fang, M.; Zhang, L. D. *Nanotechnology* **2005**, *16*, 671.
(36) Polarz, S.; Orlov, A. V.; Schüth, F.; Lu, A. H. *Chem.−Eur. J.* **2007**, *13*, 592.
(37) Yan, C. M.; Chen, Z.; Zhao, X. P. *Solid State Commun.* **2006**, *140*, 18.
(38) Zhang, P.; Xu, F.; Navrotsky, A.; Lee, J. S.; Kim, S.; Liu, J. *Chem. Mater.*, in press.
(39) Meulenkamp, E. A. *J. Phys. Chem. B* **1998**, *102*, 5566 and references therein.
(40) McMurdie, H. F.; Morris, M. C.; Evans, E. H.; Paretzkin, B.; Wong-Ng, W.; Ettlinger, L.; Hubbard, C. R. *Powder Diffr.* **1986**, *1* (2), 64−77.

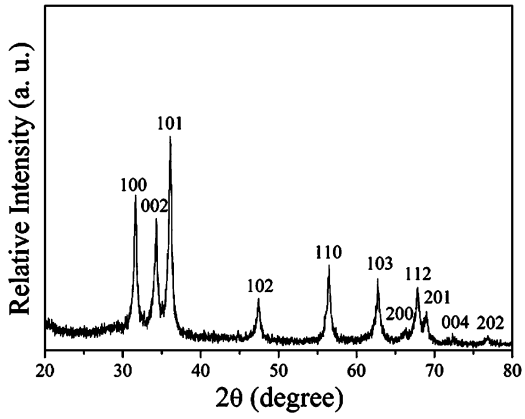

Figure 1. XRD pattern (Cu Kα radiation) of porous ZnO nanomaterials after calcination at 400 °C for 7 h.

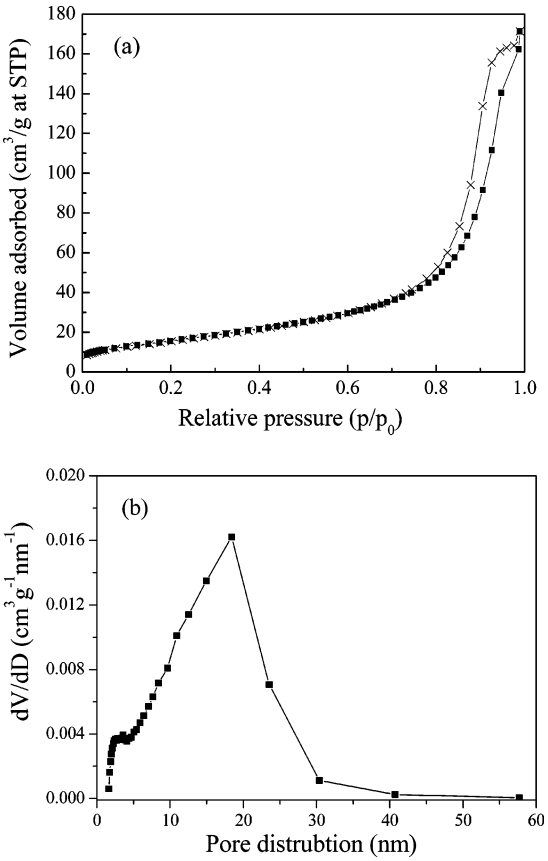

Figure 2. (a) Nitrogen adsorption−desorption isotherms for the porous ZnO nanomaterials after calcination at 400 °C for 7 h and (b) the corresponding Barrett−Joyner−Halenda (BJH) pore size distribution plot.

to the presence of large mesopores, the capillary condensation takes place at very high relative pressures and adsorption saturation is not significantly visible. The BET surface area for the calcined sample is 45.5 m^2/g, and the single-point total pore volume at $P/P_0 = 0.9894$ is 0.27 cm^3/g. Because capillary condensation occurs at relatively higher pressure, the desorption branch is used to evaluate the pore size by the BJH method. This analysis (Figure 2b) provides one narrow peak centered at ∼2.7 nm in the pore size distribution and another broad peak in the region of ∼5−30 nm with an obvious maximum at ∼18.5 nm, suggesting a dual mesopore distribution. The desorption branch also displays two distinct but less well separated steps, which suggests that two interconnected pore systems are present to form a three-dimensional pore structure.[41,42] The pores smaller than 5 nm are attributed to interconnected pores originating within individual ZnO nanocrystallites, while those large pores around 19 nm can be assigned to the interparticle space, arising from the assembly of the large individual porous ZnO particles.[1] Our porous ZnO nanoparticles have a much smaller BET surface area than samples reported by Polarz et al.[36] and Yan et al.[37] However, since there are channels in their mesoporous ZnO samples, while there are just pores rather than channels in our individual ZnO nanoparticles, it is obvious that the detailed structure is different, resulting in different surface areas.

Figure 3a is a low-magnification cross-sectional TEM image of a larger ZnO particle, confirming that this larger particle may contain many smaller ZnO nanoparticles with uniform size. The aggregation of these nanoparticles leads to the formation of the mesovoids, which may result in the generation of larger pores seen in BET analysis. Further confirmation of nanoporous structures in these smaller ZnO nanoparticles is provided by the HRTEM image of the materials calcined at 400 °C (Figure 3b), where the clear contrast difference in each individual nanoparticle shows many pores with size of about 3 nm presented. The first pore size distribution in the N_2 analysis therefore results from these nanopores. The average size of these particles estimated from Figure 3b is about 17 nm. Another HRTEM image (inset of Figure 3b) presents the lattice fringes of nanocrytallites with a spacing of 0.26 nm, which corresponds to the interplanar distance of the (002) plane of hexagonal ZnO.

Figure 4 shows a typical room-temperature PL spectrum of nanoporous ZnO materials. For ZnO, the quantum confinement effect, which could be observed from PL measurement and size-dependence of the quantum dot band gap ($E_{gap,QDs}$), can be expressed as follows:

$$E_{gap,QDs} = E_{gap,bulk} + \frac{\pi^2 h^2}{2R^2}\left(\frac{1}{m_e^*} + \frac{1}{m_h^*}\right) - 0.248E_{Ryd}^*$$

where $E_{gap,bulk}$ is taken as 3.377 eV, the bulk exciton binding energy E_{Ryd}^* is taken as 60 meV, the electron and hole effective masses are taken as $m_e^* = 0.24\ m_0$ and $m_h^* = 2.31\ m_0$, respectively, h is Planck's constant, and R is the radius of ZnO QDs.[43−45] On the basis of this equation, the exciton radius in ZnO is ∼2 nm. The average diameter of our porous ZnO nanoparticles is about 19 nm, much larger than the exciton diameter. Therefore, as a possible explanation, we suggest that PL emission from porous ZnO positioned at ∼390 nm (3.19 eV) results from the annihilation of free excitons,[46] while the emissions at ∼419 nm (2.97 eV), ∼459 nm (2.71 eV), and ∼484 nm (2.57 eV) originate from electronic transitions from the ionized oxygen vacancies to

(41) Bagshaw, S. A. *Chem. Commun.* **1999**, *18*, 1785.
(42) Yuan, Z. Y.; Blin, J.-L.; Su, B. L. *Chem. Commun.* **2002**, *5*, 504.
(43) Tan, S. T.; Sun, X. W.; Zhang, X. H.; Chen, B. J.; Chua, S. J.; Yong, A.; Dong, Z. L.; Hu, X. *J. Cryst. Growth* **2006**, *290*, 518.
(44) Kim, K. K.; Koguchi, N.; Ok, Y. W.; Seong, T. Y.; Park, S. J. *Appl. Phys. Lett.* **2004**, *84*, 3810.
(45) Kayanuma, Y. *Phys. Rev. B* **1988**, *38*, 9797.
(46) Fonoberov, V. A.; Alim, K. A.; Balandin, A. A.; Xiu, F. X.; Liu, J. L. *Phys. Rev. B* **2006**, *73*, 165317.

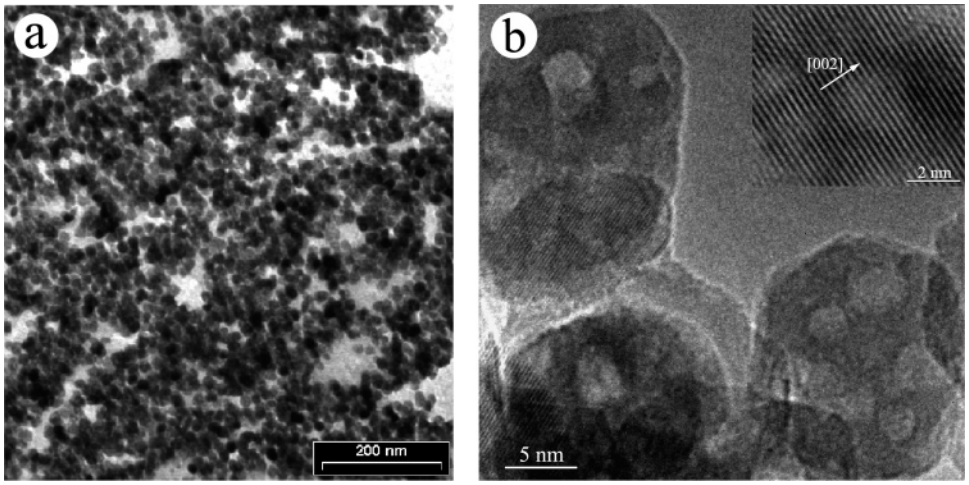

Figure 3. (a) Low-magnification cross-sectional TEM image and (b) HRTEM image of the as-obtained porous ZnO nanoparticles. The inset in part b clearly shows the lattice fringes.

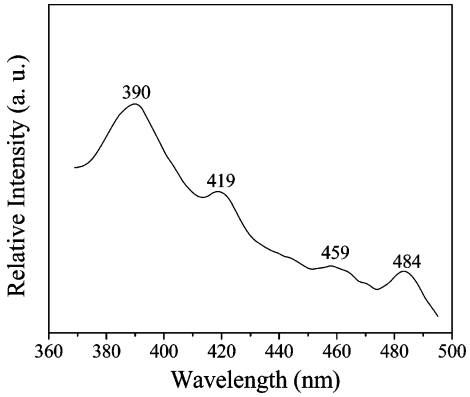

Figure 4. PL spectrum of the porous ZnO nanoparticles at room temperature ($\lambda_{ex} = 325$ nm).

the valence band.[47] This suggests that ZnO nanoporous particles may be utilized in applications of field emission.

3.2. Formation Mechanism and Role of Surface Energy. Here, we discuss, in more general terms, a versatile cooperative self-assembly route for the synthesis of porous ZnO nanoparticles, where the functionalization of the premade colloidal nanocrystallites and the copolymer surfactant templates are indispensable to form porous ZnO nanoparticles. This self-assembly process is similar to Corma's recent interpretations of the synthesis of hierarchically mesostructured CeO_2, ZrO_2, and $CeO_2-Al(OH)_3$ composites,[24] in which cooperative self-assembly of colloidal nanoparticles and a copolymer surfactant is driven by weakly attractive interaction between the surfaces of the nanoparticles and the templates. These weak interactions between the surfaces of the nanoparticles and the templates can be adjusted by effective modification of the nanoparticle surfaces; thus, this self-assembly process does not rely strongly on the specific nature of the nanoparticle building block. 2-Aminoethanesulfonic acid (taurine), the selected organic species, can satisfy such a requirement: one of the terminal groups (i.e., sulfonate) could interact specifically with the surface of ZnO, and the other terminal group (i.e., amino) would favor the interaction with the block copolymer. To better understand surface phenomena and discuss the formation mechanism, more description of the surface structure of colloidal ZnO nanoparticles is needed. As a result of specific adsorption of solutes to the surface in water, the surface chemical properties of ZnO are sensitive to the composition of the aqueous phase. So, the surface charge and pH_{zpc} are important properties of ZnO particles. In water, surface chemistry of ZnO nanoparticles is controlled by surface hydroxyl groups, which contribute to surface charge.[48] Adsorption of surfactant is also responsible for surface charge. Because the zero point of charge (zpc) of ZnO nanoparticles is at a pH of 9.3 ± 0.2,[48,49] the ZnO surface is positively charged in acidic or mildly basic media ($pH < 9$), whereas it is negatively charged under strongly alkaline condition ($pH > 9$). The low pK_a (1.5) of the sulfonic acid group of taurine ensures that this moiety can be negatively charged in a wide pH range and thus improves the interaction with the ZnO positively charged surface. $ZnO(taurine)_x$ is used to denote taurine-modified ZnO nanocolloid species (Figure 5a). P-123, as a non-ionic polymer, contains many hydrophilic (i.e., $-C-O-C-$, $-OH$) and hydrophobic (i.e., $-CH_2-CH_2-$) sites, and the polymer chain has a high flexibility because of the ease of rotation about the $-C-O-C-$ bonds. One possible conformation of P-123 chains is a compact state when concentration of polymers are much higher in an aqueous solution with a pH value of ~5, similar to the behavior of poly(methacrylic acid) in aqueous solution with $pH = 5$[50] and also that of poly(ethylene glycol) in aqueous solution.[51] This possible conformation of P-123 is shown in Figure 5b. Because there is weak attractive interaction between the tailored chemical moieties from taurine and the organic copolymer templates, several $ZnO(taurine)_x$ nanoclusters can "parasitize" on copolymer backbones (Figure 5c). Thus, copolymer P-123 directly provides a macromolecular environment for the existence of $ZnO(taurine)_x$ nanoclusters, preventing their uncontrollable coalescence. Also, there is creation of small pores (2−3 nm) in the larger ZnO

(47) Zhang, D. H.; Wang, Q. P.; Xue, Z. Y. *Appl. Surf. Sci.* **2003**, *207*, 20.
(48) Bahnemann, D. W.; Kormann, C. K.; Hoffman, M. R. *J. Phys. Chem.* **1987**, *91*, 3789.
(49) Jung, H.; Choi, H. *Appl. Catal. B* **2006**, *66*, 288.
(50) Ciardelli, F.; Tsuchida, E.; Wöhrle, D. *Macromolecule-Metal Complexes*; Springer: Berlin, 1996; pp 100−108.
(51) Xu, F.; Zhang, X.; Xie, Y.; Tian, X. B.; Li, Y. Z. *J. Colloid Interface Sci.* **2003**, *260*, 160.

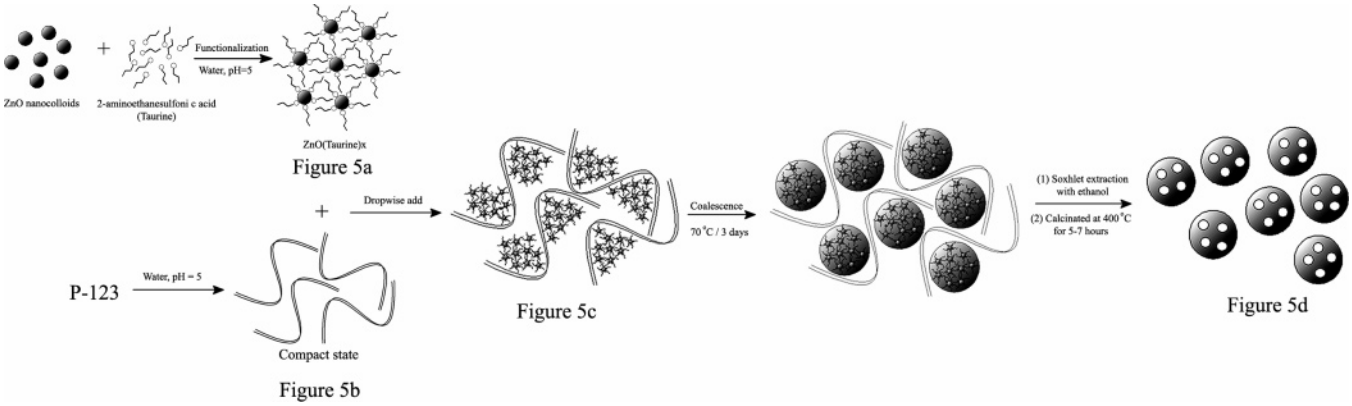

Figure 5. Schematic illustration of the self-assembly process, involving the functionalization of individual ZnO nanoparticles.

nanoparticles, after removing taurine molecules by Soxhlet extraction and calcination. As a consequence, controlled coalescence of ZnO(taurine)$_x$ nanoclusters by P-123 backbones drives the formation of uniform larger ZnO nanoparticles with interparticle spacing of ~5−30 nm, while extraction of all taurines species creates small pores of 2−3 nm in every large ZnO nanoparticle (Figure 5d). The detailed self-assembly process is illustrated schematically in Figure 5.

The fabrication of functional catalysts, nanostructures, and thick films is actually a manipulation of surface and interfacial energies. From the thermodynamic viewpoint, the combination of surface and bulk energies can provide a driving force for coarsening, size-induced transformations, and compositional changes in the interface.[52] The rapidly growing field of synthesis of ZnO nanostructures begs for experimental benchmarks of their thermodynamic properties. However, thermodynamic data for the surface energy of ZnO are rare in the literature because of the difficulty inherent in such measurements.[53,54] Recently, high-temperature oxide melt solution calorimetry has enabled the direct calculation of surface enthalpies by measuring the heat evolved on the dissolution of samples with various surface area.[52,55−57] The energetics of water adsorption on nanoparticle surfaces has also been measured for several systems.[52,56−58] Because nanoparticles in contact with their surroundings are hydrated, their energetics reflect both the surface energy of the bare surface and the hydration energy of that surface. This combined energy can be termed the surface energy of the hydrated surface, which can be measured by high-temperature oxide melt solution calorimetry. A correction is made for the water evolved during dissolution, treating the H_2O as bulk liquid water on the surface.[52,59] The resulting surface

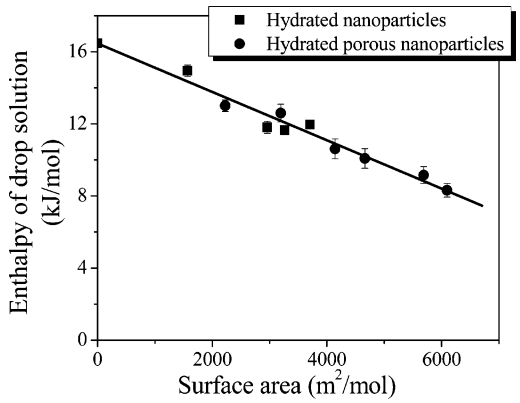

Figure 6. Enthalpy of drop solution of ZnO nanomaterials vs surface area.[38] The slope of the line corresponds to the surface enthalpy of the hydrated surface ($\gamma_{hyd} = 1.33 \pm 0.08$ J/m^2, $R^2 = 0.97$): (●) porous ZnO nanoparticles and (■) individual ZnO nanoparticles.

energy is that of the hydrated surface. The hydrated surface has a smaller surface enthalpy than the bare anhydrous surface. This thermodynamic analysis has been described in earlier papers.[52,53,56,57] Recently, we have applied oxide melt solution and water adsorption calorimetry to measure the surface energies of hydrated and anhydrous surfaces of ZnO with several morphologies, namely, nanoparticles, nanorods, nanotetrapods, and the porous assemblage of nanoparticles synthesized in this work.[38]

Figure 6 shows drop solution enthalpies ΔH_{ds} (kJ/mol) of a group of nanoporous ZnO samples and of individual ZnO nanoparticles versus the surface area (m^2/mol). The slope from a linear fit gives the surface enthalpy of the hydrated surface as 1.33 ± 0.08 J/m^2.[38] There is no difference between the nanoparticles and the nanoporous samples. The observation that the measured surface energy (for the hydrated surface) is the same in both cases suggests that contributions from interfacial energies (where particles contact one another) and from any changes in surface structure are small.[60] Thus the decrease in energy of the system is directly proportional to the decrease in surface area on self-assembly. Because the decrease in surface area is small, the driving force for such assembly, in the absence of the organics, is also small. On the other hand, P-123, an organic structure-directing agent, may convert the distribution of individual ZnO nanocrystallites to a useful set of nanocluster precursors for

(52) Castro, R. H. R.; Ushakov, S. V.; Gengembre, L.; Gouvêa, D.; Navrotsky, A. *Chem. Mater.* **2006**, *18*, 1867.
(53) McHale, J. M.; Navrotsky, A.; Perrotta, A. J. *J. Phys. Chem. B* **1997**, *101*, 603.
(54) Adamson, A. W. *Physical Chemistry of Surfaces*; John Wiley & Sons: New York, 1990; pp 313−318.
(55) McHale, J. M.; Auroux, A.; Perrotta, A. J.; Navrotsky, A. *Science* **1997**, *277*, 788.
(56) Mazeina, L.; Navrotsky, A. *Chem. Mater.* **2007**, *19*, 825.
(57) Levchenko, A. A.; Li, G.; Boerio-Goates, J.; Woodfield, B. F.; Navrotsky, A. *Chem. Mater.* **2006**, *18*, 6324.
(58) Ushakov, S. V.; Navrotsky, A. *Appl. Phys. Lett.* **2005**, *87*, 164103.
(59) Ranade, M. R.; Navrotsky, A.; Zhang, H. Z.; Banfield, J. F.; Elder, S. H.; Zaban, A.; Borse, P. H.; Kulkarni, S. K.; Doran, G. S.; Whitfield, H. J. *Proc. Natl. Acad. Sci.* **2002**, *99*, 6476.
(60) Madras, G.; McCoy, B. J.; Navrotsky, A. *J. Am. Ceram. Soc.* **2007**, *90*, 250.

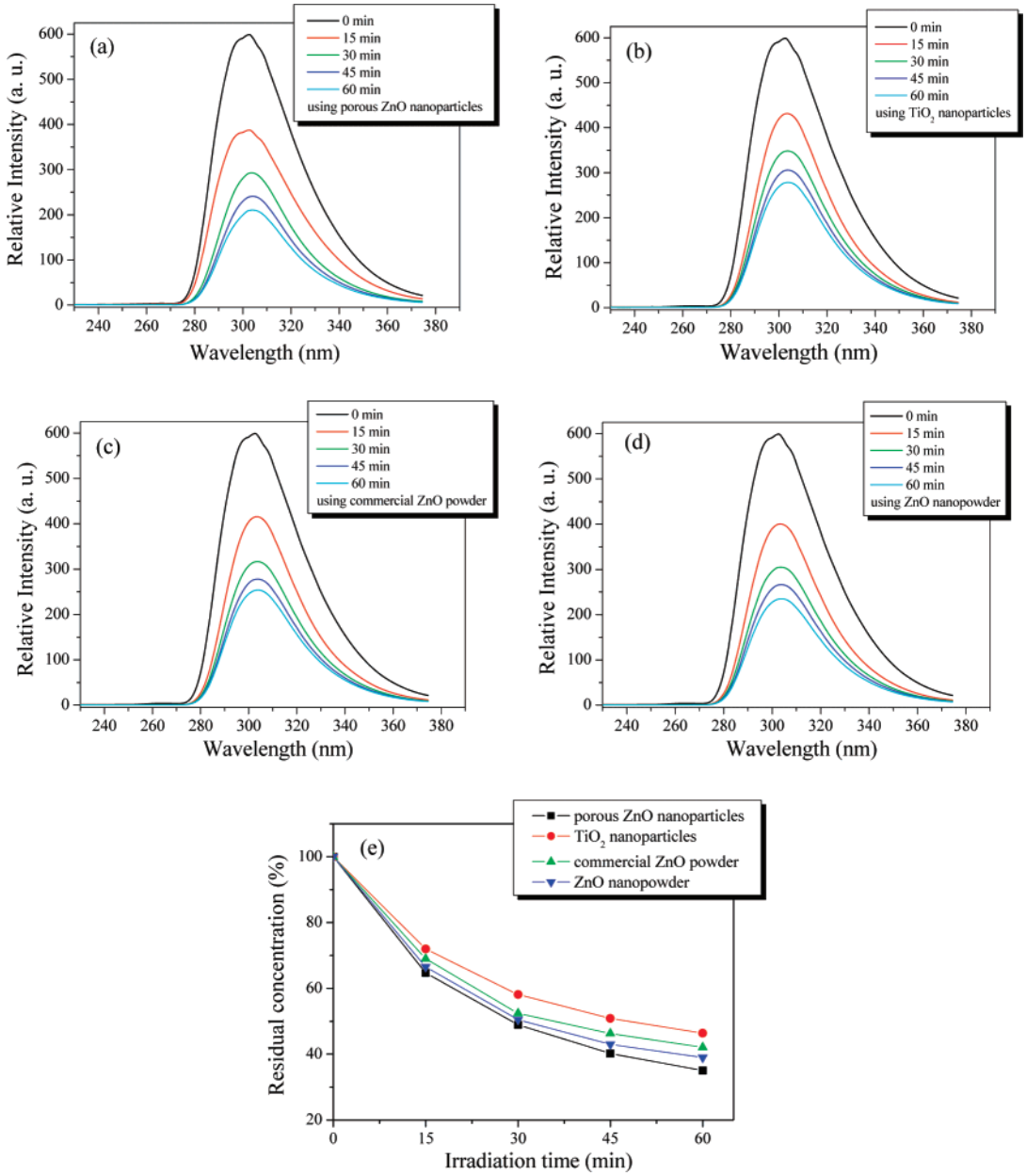

Figure 7. PL emission spectra of the residual phenol under exposure to UV light in the presence of (a) porous ZnO nanoparticles; (b) TiO_2 nanoparticles (PC-500); (c) commercial ZnO powder; and (d) ZnO nanopowder. (e) Curves of the residual fraction of the phenol as a function of UV irradiation time when using (■) porous ZnO nanoparticles, (●) TiO_2 nanoparticles (PC-500), (▲) commercial ZnO powder, and (▼) ZnO nanopowder.

assembly into the growing solid. This is similar to the role of P-123 in silica systems.[61] Organic molecules at the surface of the growing solids may increase or decrease the rate of attachment of the clusters, thus controlling shape. Also, adjusting surface charge on the growing materials, where such change can occur by adsorption of organic molecules, can control the rate of crystal growth. Here, we can envision the surfaces of colloidal ZnO nanoclusters to be positively charged by the adsorption of taurine, which favors the interaction between ZnO and P-123 polymers. This interaction at surfaces can provide the small driving force for the self-assembly process. Further, transport of ZnO nanoclusters from the "storehouse" to the growing surface will be more efficient than the transport of individual ions at low concentration.[61] Thus, nanocluster precursors, combined with organic molecules, offer a rich and controllable source of materials for both chemical synthesis and biomineralization.

3.3. Implication for Wastewater Disposal: Photodecomposition of Phenol. Phenol is a major pollutant of surface and/or groundwater, and its degradation to a safe level in the range of 0.1−1 mg/L is difficult owing to its stability and solubility in water. ZnO has been reported to be a semiconductor photocatalyst for phenol and nitrophenol degradation.[62−64] A preliminary investigation of porous ZnO materials for photocatalytic activity was performed. The characteristic PL emission of phenol at ∼300 nm was chosen

(61) Navrotsky, A. *Proc. Natl. Acad. Sci. U.S.A.* **2004**, *101*, 12096.

(62) Marcì, G.; Augugliaro, V.; López-Muñoz, M. J.; Martín, C.; Palmisano, L.; Rives, V.; Schiavello, M.; Tilley, R. J. D.; Venezia, A. M. *J. Phys. Chem. B* **2001**, *105*, 1033 and references therein.

(63) Villaseñor, J.; Reyes, P.; Pecchi, G. *J. Chem. Technol. Biotechnol.* **1998**, *72*, 105.

(64) Valenzuela, M. A.; Bosch, P.; Jiménez-Becerrill, J.; Quiroz, O.; Páez, A. I. *J. Photochem. Photobiol., A* **2002**, *148*, 177.

Table 1. Physical Characteristics of Catalysts

catalyst	porous ZnO nanoparticles	TiO_2 nanoparticles (PC-500)	commercial ZnO powder	ZnO nanopowder
surface area (m^2/g) (BET)	45.5	200−220	<3	15−25
particle size (nm)	~19	<25	500−1000[a]	<100[a]

[a] Provided by the particle manufacturer as <1000 but estimated to be >500.

as the monitored parameter for the photocatalytic degradation process. Because TiO_2 has been universally recognized as the most photoactive catalyst, we test the photocatalytic activity of TiO_2 nanoparticles (PC-500) under the same experimental conditions as for other catalysts, including commercial ZnO powder and ZnO nanopowder. Table 1 lists physical characteristics of the catalysts. Figure 7a−d shows the emission spectra of the residual phenol in aqueous solution under exposure to UV light for various times in the presence of porous ZnO nanoparticles, TiO_2 nanoparticles (PC-500), commercial ZnO powder and ZnO nanopowder, respectively. The emission peak at ~300 nm diminishes gradually as the exposure time increases and is down to <40% at an irradiation time of 60 min (Figure 7a). Figure 7e compares ZnO nanoporous materials, TiO_2 nanoparticles (PC-500), commercial ZnO powder, and ZnO nanopowder. The porous ZnO nanoparticles show superior activity to TiO_2 nanoparticles and commercial ZnO powder, as well as ZnO nanopowder. The main reason that ZnO has greater activity than TiO_2 is that ZnO absorbs over a larger fraction of UV light and the corresponding threshold of ZnO is 425 nm,[65] while the difference between porous ZnO nanoparticles and two other ZnO sources (commercial ZnO powder and ZnO nanopowder) may be attributed to the unique surface features and higher surface area.[66,67] These results indicate that porous ZnO nanoparticles have good photoreactivity in the decomposition of phenol in the wastewater.

4. Conclusion

We have developed an easy solution-based method to produce porous ZnO nanomaterials, involving the use of the taurine-functionalized colloidal ZnO particles as building blocks and a copolymer template. This method could be scaled up to large-scale production. The as-obtained products contain uniform nanopores of ~2.7 nm and a specific surface area of 45.5 m^2/g. They have better photocatalytic performance in the photodegradation of phenol than that of PC-500 titania. High-temperature oxide melt solution calorimetry has determined the surface enthalpy of hydrated surfaces of porous ZnO nanoparticles to be 1.42 ± 0.21 J/m^2, consistent with that of isolated ZnO nanoparticles. The calorimetric results interpret this versatile cooperative self-assembly strategy, where the interaction between a copolymer template and an organic moiety through a surface modification of nanocrystallites can be utilized to form nanoporous materials.

Acknowledgment. This research was supported by DOE Grant DE-FG0301ER15237. F.X. also thanks University of Namur (FUNDP) for a postdoctoral research fellowship.

CM071190G

(65) Behnajady, M. A.; Modirshahla, N.; Hamzavi, R. *J. Hazard. Mater. B* **2006**, *133*, 226.

(66) Tian, Z. R. R.; Voigt, J. A.; Liu, J.; McKenzie, B.; McDormott, M. J.; Rodriguez, M. A.; Konishi, H.; Xu, H. F. *Nat. Mater.* **2003**, *2*, 821.

(67) Xu. F.; Yuan, Z. Y.; Du, G. H.; Ren, T. Z.; Bouvy, C.; Halasa, H.; Su, B. L.; *Nanotechnology* **2006**, *17*, 588.